Journal of Medical and Biological Engineering
https://doi.org/10.1007/s40846-022-00740-5

ORIGINAL ARTICLE

DXA-Based Finite Element Analysis as Support for Pre and Post-operative Evaluation of Hip Arthroplasty

Sofia Cuttone[1] · Luca Rinaudo[1] · Cristina Bignardi[2,3] · Alessandra Aldieri[4,5] · Mara Terzini[2,3] · Antonio Croce[6] · Carmelo Messina[6] · Laura Mangiavini[6,7] · Luca Maria Sconfienza[6,7] · Fabio Massimo Ulivieri[8]

Received: 9 May 2022 / Accepted: 1 July 2022

Abstract

Purpose Bone quality, bone density, implant type and patient anatomy are critical factors for the success of Total Hip Arthroplasty. This study aims to develop a patient-specific FE model based on DXA images to optimise preoperative planning and follow-up.

Methods Three simulations were carried out for each patient: intact femur, press-fit stem and cemented stem, selecting different prosthesis sizes and types (cemented and cementless). The loads were applied at the centre of the femoral head, whereas constraints were placed on the distal nodes of the femoral shaft to simulate the walking condition. The mechanical response was assessed through micromovements, equivalent strains and strain energy density (SED) calculation.

Results Models with press-fit prostheses show an average strain greater than 20% compared to the intact femur and 10% compared to models with cemented prostheses. Femoral average strain ranged from about 600 to about 1500 μstrains depending on the patient BMI, BMD and type of implant. The femoral prosthetic models show the highest strain values in Gruen zones located medio-proximally, and lower strains in the lateral regions, mainly for cemented implants. The SED follows the same trend as the average equivalent strain in the Gruen zones.

Conclusion DXA-based FE analysis appeared to be helpful to access bone strain distribution in prosthetic hip depending on patient anatomy, BMD, and the type of implant. The study shows the utility of equivalent strains and strains energy density in predicting bone loss and growth around the prosthesis and the influence of BMD and BMI in the final results.

Keywords DXA · Total hip arthroplasty · Finite element analyses · Patient-specific modelling · Prostheses

1 Introduction

Total hip arthroplasty (THA) provides excellent pain relief and amelioration in functional capacity. It improves the objective performance scores in patients with debilitating *functio laesa* of the hip joint affected by osteoarthritis [1]. Even though differences exist in the number of THA procedures performed across the different Countries, approximately one million hips are replaced by prostheses worldwide each year. The hip replacement rate increased by 25% between 2000 and 2009 [2]. Therefore, despite improvements in prosthesis material, design and implantation procedures that led to a reduction in the percentage of failures, the absolute number of failed joints has increased dramatically. Data from national registries provide clear statistics of failure rates, but the failure mechanisms are often still unclear and a matter of discussion.

In a successful hip replacement procedure, preoperative planning is a crucial step. It is carried out through several stages: anamnesis and acquisition of the patient's clinical history; radiological investigations; assessment of the patient's suitability for surgery; choice of the best implant for the specific individual case.

Commonly, preoperative planning is done by superimposing the prosthesis model on hip radiographs using digital models. The modelling process guides the surgeon in choosing the prosthesis size and in estimating the optimal positioning and depth of insertion of components. [1]. This procedure considers only the geometry of the bone subjected to the implant without considering the information related to bone density or the load to which the implant will be subjected. Nevertheless, the long-term implant stability also

✉ Fabio Massimo Ulivieri
ulivieri@gmail.com

Extended author information available on the last page of the article

Published online: 10 August 2022

depends on the load transmission to the adjacent bone, which is therefore not currently taken into account during preoperative planning [3]. A load transfer that strongly deviates from the physiological bone loads might can cause stress-shielding, bone resorption, or fibrous tissue growth due to excessive micro-movements at the implant-bone interface [4]. The load transfer from implant to bone is also affected by the type of implant selected, e.g., cemented or cementless. Depending on the type of implant and the strategies used for prosthesis fixation, bone cement can cause a reduction in bone density due to the removal of physiological stress from the bone, leading to the weakening of the bone in that area [5]. Conversely, in the case of non-cemented stems based on press-fit, the preloading of bone layers immediately adjacent to the stem ensures primary stability, which is a prerequisite for bone formation [5]. At present, non-cemented implants commonly represents the preferred and most spread choice [5].

In this context, a patient-specific analysis of the bone density distribution, bone geometry, and loads exchanged between the femur and the implant might provide insights into the currently missing information, allowing more accurate analysis of the overall clinical situation and enhanced preoperative planning. Patient-specific Finite Element (FE) analyses might represent, in this perspective, a powerful tool to support clinicians and surgeons in achieving this ambitious goal [6]. Over the past 50 years, FE analyses have been used in orthopaedics biomechanics and have grown in size, sophistication and techniques to assess the postoperative mechanical environment. FE can support the understanding of the mechanical behaviour of orthopaedic devices and guide the decision-making process of the orthopaedic surgeon, dealing with many aspects of an implant, such as wear, cement or implant-bone interface and damage accumulation osseointegration [6]. FE models informed by computed tomography (CT) imaging have been adopted in several contexts, ranging from bone fracture risk prediction [7, 8] to selection of the appropriate surgical procedure [4]. The role of CT-based FE models employed to improve the outcome of a hip replacement procedure has already been explored [3, 4, 6]. Nevertheless, the preoperative planning of a hip replacement surgery is still far from being supported by patient-specific CT-based FE models. Because of CT-associated high radiation dose and costs and the relatively high computational efforts related to CT-based FE analyses implementation, their adoption is still impractical in the clinical workflow [9–11]. Beyond CT-informed FE models, also Dual X-rays Absorptiometry (DXA)-informed FE models have been studied and their role investigated in the fracture risk prediction [12]. DXA produces a two-dimensional image which represents the projection of the three-dimensional structure of the femur. DXA involves negligible radiation dose and decreased costs and is a technique routinely used in the clinical setting. Although due to DXA inherent projective nature, a DXA-based FE model is less accurate than a CT-based one [13], it would require lower computational cost and time, which is more compatible with the clinics [14].

Therefore, this study aimed to investigate the role of two-dimensional FE models built from DXA scans in supporting the preoperative planning and the follow-up of hip arthroplasty.

With this aim, patient-specific DXA-derived FE models were developed for twenty patients. For each patient, FE analyses were conducted considering the intact femur and subsequently inserting two different types of hip stems (cemented and cementless) in nine different sizes. Bone strains were computed across the 7 Gruen areas around the implant and the outcomes from the implanted femur model compared to those obtained from the intact femur model.

2 Methods

The study was conducted starting from the DXA images of twenty patients, six male and fourteen female subjects, all between 53 and 86 years of age (Table 1), randomly chosen from a completely anonymised dataset from a previous study [15]. In order to simulate the lengths of different prostheses, each scan was virtually modified to maximize the available femur portion by repeating the last scan line at the base of the femur. Hip structural analysis (HSA) parameters were extracted with APEX 3.3 DXA software for the whole cohort. Two-dimensional geometries of non-cemented and cemented straight stems (Korus), with caput-collum-diaphyseal (CCD) angle equal to 135° and 125°, had been made available by Gruppo Bioimpianti, Peschiera Borromeo, Milan, Italy.

2.1 Two-Dimensional Model Construction

Two-dimensional geometric models of the femur were built by segmenting the available DXA images through an automatic segmentation procedure (Matlab v2021a, MathWorks Inc.). For each patient, three distinct models were generated: (1) the intact femur (Fig. 1a), (2) the femur with the cementless stem inserted (Fig. 1b), and (3) the femur with the cemented stem inserted (Fig. 1c). The

Table 1 Mean and standard deviation of age, height and weight of the six males and fourteen females in the study [15]

	No. patients	Age	Height [cm]	Weight [Kg]
Males	6	64 ± 11	168.7 ± 6.2	73.4 ± 8.6
Females	14	69 ± 9	159.6 ± 7.3	58.5 ± 9.2

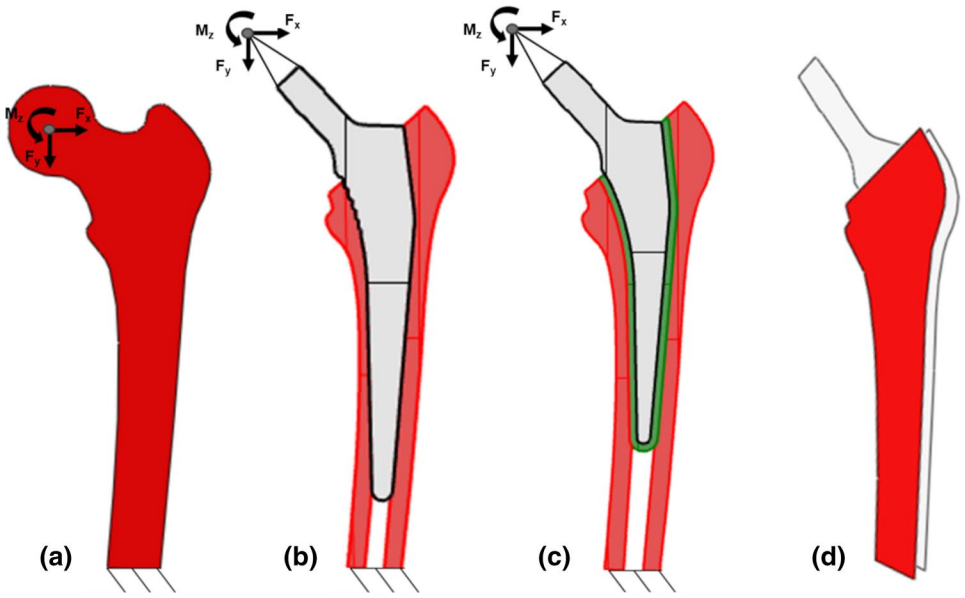

Fig. 1 **a** 2D models and boundary conditions: the intact femur, **b** femur with cementless stem, **c** femur with cemented stem [the cement uniform layer (3 mm thickness) is shown in green], **d** side plate

virtual stem insertion in the femur was carried out according to the procedure detailed in the following. First, different stem sizes fitting the two-dimensional geometry of the medullary canal were selected by visual inspection and checked by an expert surgeon. Then, the starting geometry of the intact femur was cut through Boolean operations so that the stem could be inserted into it.

Uncemented models were characterized by:

- Stems made of titanium alloy TI-6Al-4 V [16, 17];
- A 50 µm reduced medullary canal in order to create an interference fit to model the press-fit action [18].

Cemented models instead were characterized by:

- Stems made of high nitrogen content stainless steel [19];
- A uniform layer of Polymethylmethacrylate (PMMA) of the same shape as the implant, 3 mm thick between the bone and the prosthesis [20].

2.2 Finite Element Models

After the creation of the geometric model, the FE models were built. Due to the two-dimensional nature of the model, the femur and implant were modelled as plates with constant thickness. Following a mesh convergence analysis, FE meshes were generated using 6-node triangular plane stress elements with a dimension of 0.3 mm for both prosthesis and bone (HyperMesh2019, Altair Engineering). FE simulations were performed in Abaqus (v6.13, Simulia, Dassault Systèmes, Providence, RI) under static loading conditions.

2.2.1 Intact Femur

The thickness of the intact femur FE model was determined patient-specific, based on the HSA femoral neck width [21]. More precisely, it was calculated so that the cross-section area and moment of inertia matched those of a circular cross-section at the femoral neck [12].

Local Young's moduli (E) of the bone were derived using the empirical relationships developed by Morgan et al. [22]:

$$E(MPa) = \begin{cases} 15010\rho_{app}{}^{2.18} if\, \rho_{app} \leq 0.28 gcm^{-3} \\ 6850\rho_{app}{}^{1.49} if\, \rho_{app} > 0.28 gcm^{-3} \end{cases} \quad (1)$$

where ρ_{app} is the apparent density, calculated from the patient-specific thickness and the values of local Bone Mineral Density (BMD) [21]. For the material properties assignment, the elements were grouped into 55 bins according to their BMD value; based on the median BMD value of each bin, the corresponding Young's modulus was then calculated and assigned to all the elements of the bin [12]. The number of bins was identified following a convergence analysis.

2.2.2 Implanted Femur

The hip stem is surrounded by bone when implanted in the actual situation. When modelling this situation with a two-dimensional model, the three-dimensional contribution of the bone needs to be taken into account, otherwise, the two sides of the 2D model of the bone will tend to open in the presence of the stem, which is unrealistic. Hence, to simulate the structural contribution of the cortical bone and its

three-dimensional connectivity, the implanted femur models included three components: the femur, the stem and a side plate, which was added according to Gonzalez et al. [23] to keep the two lateral parts of the femur surrounding the stem connected together. The side plate, linked to the bone, had the same geometry as the femoral model and connected the medial and lateral cortical bone (Fig. 1d). The side plate element size was set to 0.5 mm, since only its structural contribution mattered. The thickness of the side plate was assumed to be constant and equal to 2 mm. The one for the implanted femur was the differences between the fixed side plate and the intact femur thichness. The thickness of the implant stem was set equal to 4 mm, except for the neck, whose thickness was considered equivalent to 6 mm [24]. The Young's Modulus of the side plate was assumed to be equal to the average bone Young's modulus. A Young's modulus of 110 GPa was assigned to the cementless stem [16, 17], while a Young's modulus of 195 GPa was assigned to the cemented stem [19], and the value assigned to the glue was equal to 220 MPa [25]. The Poisson's ratio, in all cases, was considered equal to 0.3.

In the case of the cementless hip stem, a node to surface contact was set between the bone and the stem, with friction coefficient equal to 0.3 [26]. In the case of the cemented stem instead, however, the cement was fully bonded to the bone [17], while frictional contact was set between stem and cement with friction coefficient set to 0.5 [26].

2.2.3 Boundary Conditions

Moments and forces related to the most critical moment of the walking cycle were applied, as obtained by Heller et al. [27]. Loads were given as a % of the patient's Body Weight (% BW) and could therefore be applied in a patient-specific way. In particular, the components of the force along the mediolateral axis (x-axis) were calculated as 6.51%BW, the component along the longitudinal axis (y-axis) was calculated as 76.98%BW, and the moment around the anteroposterior axis (z-axis) was considered equal to 5.163%BW. As shown in the case of the intact femur, the loads were applied at a reference point placed at the centre of the femoral head, which was kinematically coupled to all the nodes of the femoral head (Fig. 1a). In the implanted femur, the loads were applied to a reference point analogously constrained to the nodes of the upper edge of the implant neck (Fig. 1b, c). The distal nodes of the femur were constrained in all directions, and the medial and lateral nodes were connected to those of the side plate through a "Tie" constraint.

2.3 Evaluation of Mechanical Response

Three quantities were used to assess the mechanical response of the 2D models: the micromovements at the stem-bone and stem-cement interface [18, 28, 29], the equivalent strain [14] and the Strain Energy Density (SED) [30]. The first is usually used as an indicator of interfacial failure, aseptic loosening of prosthetic components or bone growth [18, 28, 29]. More in detail, micromotions of the stem in the bone and cement were evaluated using the tangential (CSLIP) and normal displacements (COPEN) for each node (n) in the contact surface according to the following relationship:

$$Micromotions(n) = \sqrt{[CSLIP(n)]^2 + [COPEN(n)]^2} \quad (2)$$

The average micromotion value was extracted for each patient's simulated stem size. The equivalent strain provides information about the mechanical deformation of the bone subjected to a load, and the SED is commonly used as an indicator of bone resorption stimuli [30]. In particular, based on results on micro-motion, a prosthesis size was chosen for each patient, and the two variables were extracted for the patient-specific intact femur, cemented femur, and cementless femur models. The element-by-element relative difference computed for the equivalent strain between the implanted and femur was calculated. The equivalent strain and SED per Gruen zone of fourteen female patients and six male patients were averaged. Finally, the average equivalent strain for normal, osteopenic and osteoporotic female patients and the average equivalent strain for underweight, normal weight and overweight female patients were evaluated.

3 Results

3.1 Micromotions

Figure 2 shows the average micromotions distribution for a subgroup of ten femur models with different uncemented and cemented stem sizes. For models with press-fit prostheses, the micromotions at the bone-stem interface decrease as the size of the prosthesis increases; this trend, instead, is less evident at the cement-cemented stem interface.

3.2 Equivalent Strains

The mean equivalent strain for the female patients in the three different patient-specific models was evaluated as a function of Body Mass Index (BMI) and T-score. The mean equivalent strain increases as the BMI increases (Fig. 3). For all BMI values, models with press-fit prostheses show, on average, a strain greater than 20% compared to the intact femur and 10% compared to models with cemented prostheses. Instead, the latter have a mean equivalent strain 5% higher than the intact femur for BMI < 18.5 and 10% for BMI > 18.5. Figure 4 shows the mean equivalent strain as

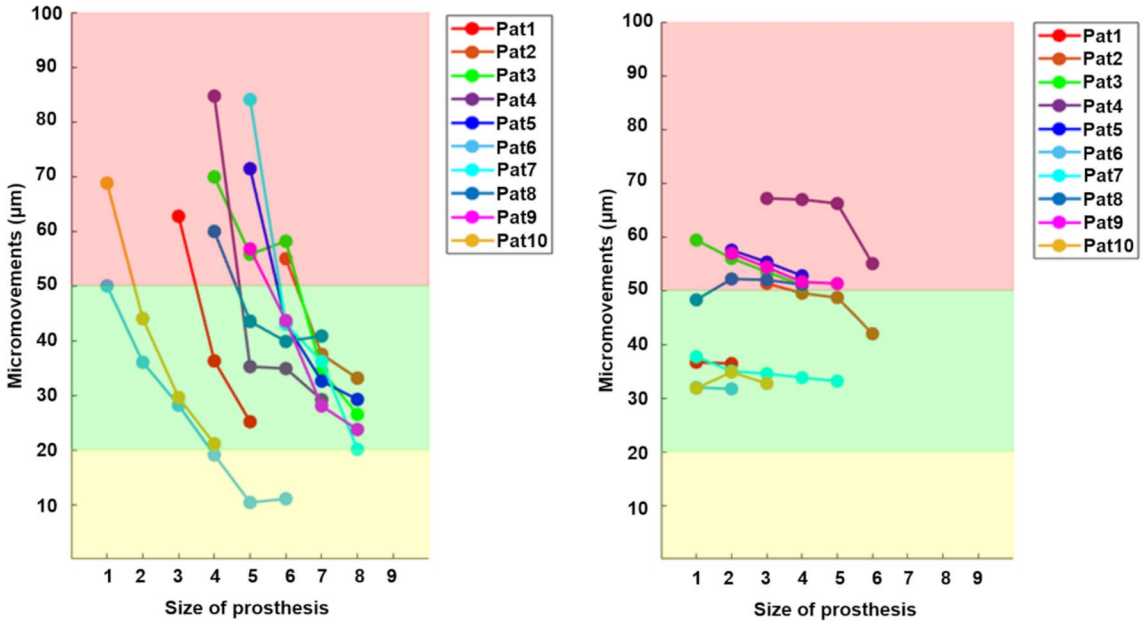

Fig. 2 Shows the average micromotions distribution for a subgroup of ten femur models with different uncemented and cemented stem sizes. For models with press-fit prostheses, the micromotions at the bone-stem interface decrease as the size of the prosthesis increases; this trend, instead, is less evident at the cement-cemented stem interface

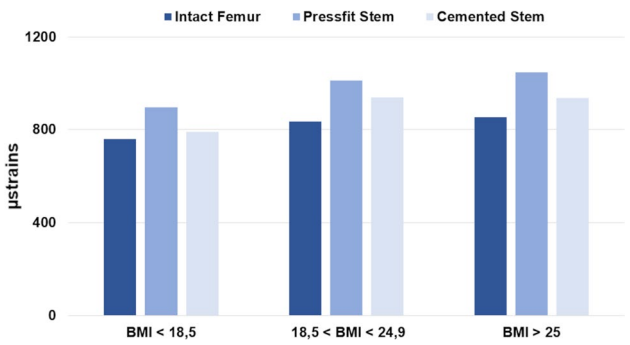

Fig. 3 Average equivalent strain (µstrains) for the intact femur, femur with press-fit stem and femur with cemented stem for underweight (BMI ≤ 18.5), normal weight (18.5 < BMI ≤ 24.9) and overweight (25 ≤ BMI ≤ 29.9) female patients

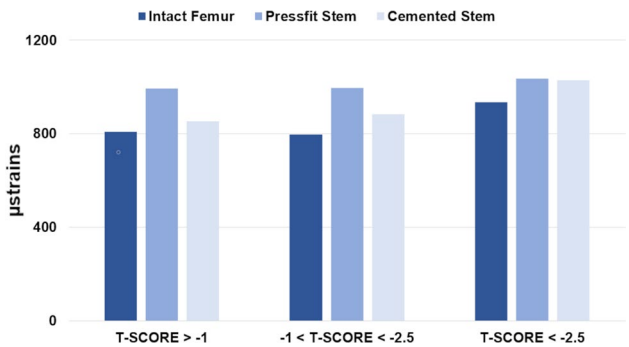

Fig. 4 Average Equivalent Strain (µstrains) for intact femur, femur with press-fit stem and femur with cemented stem for normal (T-SCORE > − 1), osteopenic (− 1 < T-SCORE ≤ − 2.5) and osteoporotic (T-SCORE < − 2.5) female patients

a function of the T-score for female patients. Osteoporotic patients (T-score < − 2.5) are subjected to greater strains than osteopenic (− 1 < T-score < − 2.5) and normal patients (T-score > − 1). In particular, for all T-score classes, the intact femur has minor equivalent strains compared to implanted models. Uncemented prostheses generate equivalent strains higher than 950 µstrains; cemented prostheses produce equivalent strains of approximately 850 µstrains for T-score > − 2.5 and higher than 950 µstrains, in analogy with press-fit models, for T-score < − 2.5.

Figure 5 shows the average equivalent strains for the female patients in the seven Gruen zones (Fig. 6a) for the intact and implanted femur. In zones 1 and 2, located

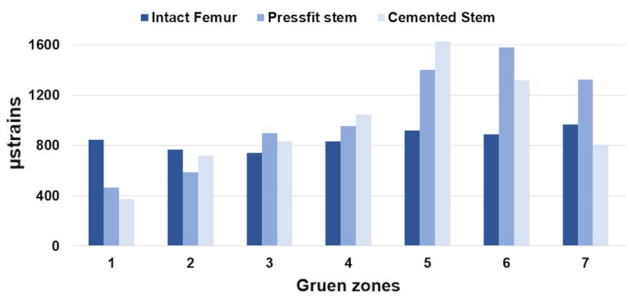

Fig. 5 Average equivalent strain (µstrains) for the intact femur, femur with press-fit stem and femur with cemented stem per Gruen zones for the fourteen female patients

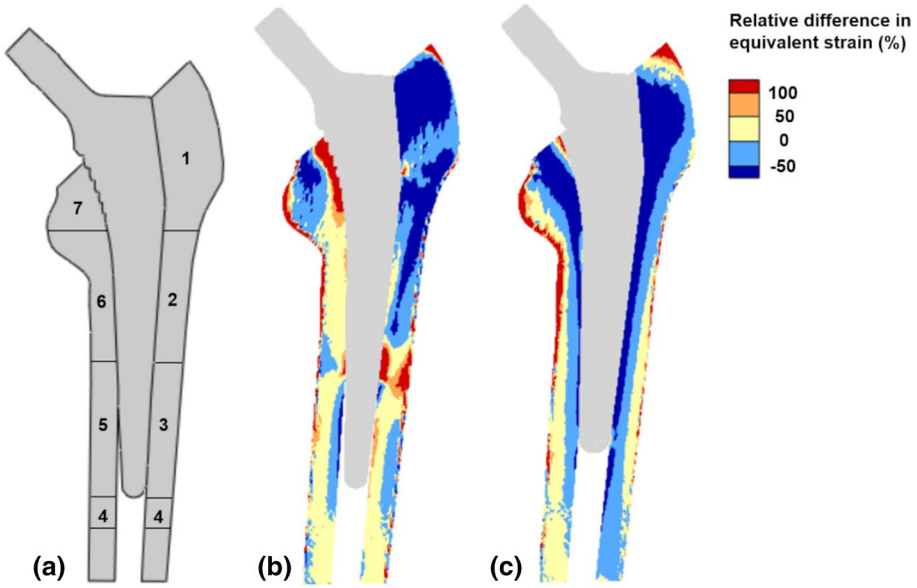

Fig. 6 **a** Gruen zones, a relative element-by-element difference of equivalent strain compared to the intact femur for patient nine: **b** model with a press-fit prosthesis and **c** model with a cemented prosthesis

proximally and laterally, the models with press-fit and cemented prostheses show strains lower than the physiological ones; in zone 3, strains reach values of about 800 μstrain, slightly higher than the intact femur. Cemented prostheses generate more significant strains in the intact femur and the non-cemented models in zone 4, located distally, and 5, located medio-distally, where a maximum of 1600 μstrains for women are reached. In zone 7 instead, they turn out to be lower. Models with press-fit prostheses show the highest strain values in zones 6 and 7, located medio-proximally. Still, they are generally characterised by more significant strain levels than the intact femur in all zones, except zones 1 and 2. The strains measured in the male subgroup follow the same trend but have lower absolute values compared to the female subgroup.

Furthermore, the models with press-fit and cemented prostheses were compared with the intact femur. The distribution of the element-by-element relative differences between the equivalent strains of the implanted and intact femur models are consistent with the mean results. Looking at Fig. 6b and c, which depict results relative to only one of the twenty patients, negative relative differences indicate areas where the equivalent strains are less than in the intact model; on the contrary, positive differences are attributable to higher equivalent strain values.

Cemented femurs do show more elements characterised by subnormal strains than press-fit models. In particular, as shown by Fig. 6c, Gruen zones 1, 2, 3 and 7 are not physiologically loaded and display negative differences. The strains are very low in the areas near the inner femoral edge, in contact with the stem, and increase progressively moving away from it. The most significant differences concerning press-fit models are observed in zones 6 and 7, where the cemented prostheses have 50% decreased strains compared to the intact femur. Non-cemented models, on the other hand, show reduced strains compared to the intact ones in the proximal lateral zones 1–2 and the highest number of elements with positive relative differences in zone 6. However, unlike cemented models, the implant-bone load transfer is not homogeneous. Very high relative differences (100%) are found in zone 7, where the transferred load is more significant, as well as in locations where the bone-implant contact ends, located more or less distally depending on the size of the prosthesis. These strain peaks, not being homogeneously distributed, are followed by areas showing relative negative differences.

3.3 Strain Energy Density

Figure 7 shows the mean SED values for the intact femur, femur with press-fit stem, and femur with cemented stem

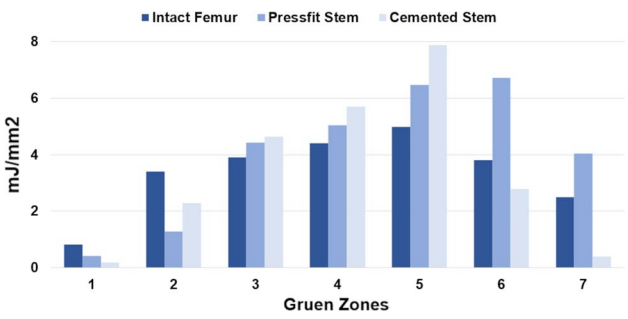

Fig. 7 Average strain energy density (mJ mm^{-2}) for the intact femur, femur with press-fit stem and femur with cemented stem per Gruen zones for the fourteen female patients

models, respectively for each Gruen zones. The SED follows the same trend as the average equivalent strain in the seven Gruen zones. In the press-fit stem models, the SED is lowest in zone 1 (0.50 mJ mm^{-2}) and has the maximum value of 6.73 mJ mm^{-2} in zone 6. In zone 2, the cementless stem models produce a decreased SED (negative differences), equal to 1.28 mJ mm^{-2}, compared to the intact femur models (3.40 mJ mm^{-2}). As already highlighted by the equivalent strain, the most significant differences occur medio-proximally in zones 6 and 7, where the SED values are significantly higher than in the intact femur. In the cemented models, the SED is higher in the distal Gruen zones (3, 4, 5) with a maximum value in zone 5, equal to 7.98 mJ mm^{-2}; on the other hand, SED is lower (negative differences) in zones 1, 2, 6 and 7. Zone 7 shows the highest difference compared to the intact femur, corresponding to − 84.8%. As already observed for the equivalent strain, the SED values measured in the male subgroup follow the same trend but have lower absolute values than the female subgroup.

Figure 8a and b show the distribution of the elements where bone growth ($SED_{prosthetic} > SED_{femur}$) or bone resorption ($SED_{prosthetic} < SED_{femur}$) might seem fostered for the cemented and uncemented models of patient 9. The areas suggesting bone resorption (in blue) coincide with those where relative differences computed for the equivalent strain are negative, while positive differences characterise the areas of supposed bone growth (in red). Figure 8a shows that press-fit stem models are characterised by SED values greater than those obtained in the medial areas of the intact femur models. Figure 8b shows that cemented stem models are characterised by SED values greater than the intact femur models in medial-distal areas. Typically, both stem models display lower SED values than the intact model in the lateral areas. Still, cemented models show more elements

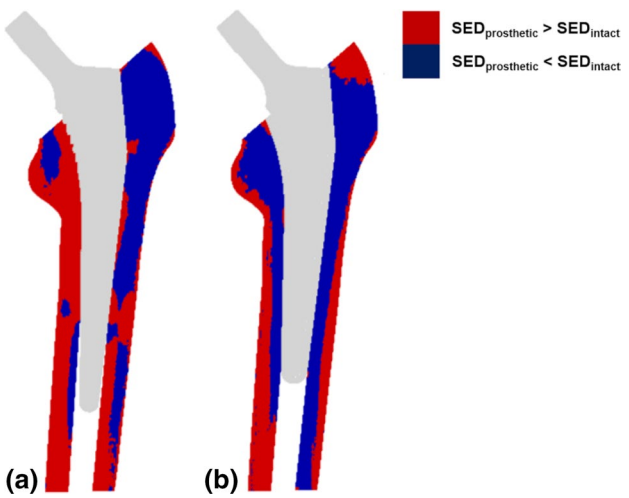

Fig. 8 Strain energy density for patient nine: **a** model with a press-fit prosthesis and model with a cemented prosthesis (**b**)

with lower SED values than cementless stem models and, therefore, might seem to suggest bone loss according to the remodelling theory of Huiskes et al. [30].

4 Discussion

In light of the progressive increase in THA and revision surgeries related to implant failure in recent years, the need for more accurate preoperative planning and dedicated follow up has become more and more evident. A factor that influences the success of hip replacement surgery is the mechanical quality of the bone. It has been shown that short medium-term outcomes are significantly influenced by bone mineral density and body mass index [31]. Subjects with osteoporosis may undergo periprosthetic fractures or prosthesis mobilisation due to the low mechanical resistance of the bone to the loads to which it is subjected [31]. In addition, subjects with low preoperative BMD show a greater bone loss in the areas around the implant in the months following the surgery [32]. Therefore, surgery planning could be enhanced if functional, biomechanical and anatomical informations were considered. Despite the spreading of CT-based patient-specific FE models in the last decades, they are currently not part of the standard preoperative planning procedure, mainly because of CT related costs and dose. Due to the above considerations, this work focused on developing DXA-informed FE models in THA preoperative planning and subsequent follow up. DXA could indeed more easily be performed, and FE models informed by DXA images might be more straightforwardly integrated into the current clinical practice. Therefore, the goal of this study was to explore how informative DXA-based patient-specific FE models could be and to know the extent they were able to capture differences between different hip stem types and sizes. The analysis of the micro-movements at the bone-implant interface allowed identifying the most suitable size for the patient to promote bone growth and inhibit the formation of fibrous tissue [6, 28, 29]. Furthermore, comparing the equivalent strain values and the strain energy density between the different models allowed us to assess which regions of the femur were more affected by the implant presence in relation to patient anatomy, BMD, and the type of implant used.

Heavier and osteoporotic patients seem subjected to major bone strains since the average equivalent strain levels increase with increasing BMI and decreasing T-score. This is consistent with the literature [14] and with the physical considerations that correlate higher BMI with higher forces acting on the bone and higher bone density with stiffer material properties. Observing the equivalent strain distribution in the seven Gruen zones described in Fig. 5, the uncemented stem models reported lower values with respect to the intact femur only in the proximal lateral areas 1 and 2.

In contrast, they exhibited higher values in proximal medial regions 5, 6 and 7. On the other hand, the equivalent strain calculated in the case of press-fit implants appeared to be higher in medial proximal regions 6 and 7 and lower in the distal areas 4 and 5 compared to cemented stem models.

The equivalent strain distributions obtained from the presented analysis are in accordance with literature results [29, 33], especially because press-fit prostheses are able to preserve higher strain levels medially in the proximal femur regions compared to the cemented solution.

The FE analysis performed in this study showed how the implant presence affects the strains in the areas adjacent to the stem and transfers the loads distally. This phenomenon, called stress shielding, causes bone resorption of the cortical bone around the stem and the BMD decrease due to subnormal stresses [34]. The press-fit stem preloads the areas adjacent to the implant, promoting bone growth and osteointegration. These results are confirmed by the SED distribution, which showed higher values for this kind of stem, except for Gruen zones 1 and 2. On the other hand, cemented implants appear to lead to bone loss, especially in zone 7, where SED is 90% lower than in the intact femur. This might also be due to the greater rigidity of the cemented stem [35].

Overall, this work highlights the influence of BMD, BMI, implant design and surgical approach on the femoral strain state. Furthermore, the results show the usefulness of DXA-based FE analysis in predicting bone loss or bone growth around the prosthesis that can define the long-term outcome of the surgical intervention. In fact, it is essential to anticipate the onset of any complication in the postoperative period. In this scenario, this type of analysis could help in predicting bone resorption and formation in DXA post-operative evaluation, anticipating BMD values of the following DXA examinations and providing more time for drug treatment or new surgical procedure intervention.

Major discrepancies arising from the comparison between the intact femur and press-fit models might have been affected by the way the implant has been inserted into the femur through Boolean operation and how prosthetic femurs have been simulated. Further validation and comparisons with taking advantage of DXA scan follow-up will be needed.

From this perspective, this study is mainly limited by the fact that it is based on virtually modified images and by the unavailability of follow-up information. The possibility to compare the model's predictions with data coming from follow-up images will allow to assess the credibility and reliability of the presented approach. A clinical study is actually being planned, which will be useful in validating and assessing the actual potential of the presented framework. In addition, only one possible design of the stem was tested, although the authors are aware of the fundamental role the implant design plays in the determination of bone strain and stress distribution. Nonetheless, it must be noted that the presented framework is applicable to any implant design, both in press-fit and cemented configurations. Following the planned clinical validation study, the next step would be the automatization of these FE analyses within existing software (e.g., Bone Strain Index [36]). In this way, the overall preoperative planning procedure will be considerably enhanced, and the prediction of performances might be even further improved thanks to the possibility to integrate the results optained with additional patient-specific decision tools, such as that provided by English National Joint Registry (NJR) [37].

5 Conclusion

Given the increase in prosthetic interventions and the need to anticipate possible failures, to date, DXA-based FE analysis could guide the management of preoperative planning of THA and subsequent follow-up, providing information currently missing. Through a two-dimensional DXA-derived FE analysis, it is possible to evaluate the choice of the implant and the surgical approach best suited to the patient, taking into account factors such as the geometry and strength of the bone, the load to which the implant is subjected and the consequent distribution of the bone strain. The proposed FE analysis approach could facilitate and improve the clinical management of the patient. Furthermore, given the high presence of DXA devices on the territory, the presented approach could represent an optimal solution for patient follow-up with analysis times and execution costs suitable for its use in clinical practice.

Funding The authors declare that no funds, grants, or other support were received during the preparation of this manuscript.

Declarations

Conflict of interest The authors have no relevant financial or non-financial interests to disclose.

Ethical Approval This study was based on the DXA images of twenty patients randomly chosen from a completely anonymised dataset coming from a previous study [15]. This previous study, entitled "*A new finite element based parameter to predict bone fracture*" and published on December 5, 2019, has obtained the approval of the Local Ethical Committee: Comitato Etico Milano Area 2. Protocol N 2.0 BQ. 265_2017, 13th June 2017.

Consent to Participate Informed consent was obtained from all individual participants included in the study.

References

1. Shaikh, A. H. (2018). Preoperative planning of total hip arthroplasty. In V. Bagaria (Ed.), *Total hip replacement*. Rijeka: IntechOpen. https://doi.org/10.5772/intechopen.76368

2. Holzwarth, U., & Cotogno, G. (2012). *Total hip arthroplasty : State of the art, prospects and challenges*. Luxembourg (Luxembourg): Publications Office of the European Union. Retrieved May 31, 2022, from https://publications.jrc.ec.europa.eu/repository/handle/JRC72428
3. Dick, C., Georgii, J., Burgkart, R., & Westermann, R. (2008). Computational steering for patient-specific implant planning in orthopedics. In *VCBM* 2008 *First EG Workshop on Visual Computing for Biology and Medicine.* https://doi.org/10.31729/jnma.634
4. Reggiani, B., Cristofolini, L., Varini, E., & Viceconti, M. (2007). Predicting the subject-specific primary stability of cementless implants during pre-operative planning: Preliminary validation of subject-specific finite-element models. *Journal of Biomechanics, 40*(11), 2552–2558. https://doi.org/10.1016/j.jbiomech.2006.10.042
5. Mario Izzo, G. (2012). Support for total hip replacement surgery: Structures modeling, Gait Data Analysis and Report system. *European Journal Translational Myology-Basic Applied Myology, 22*(2), 69–121. https://doi.org/10.4081/ejtm.2012.1795
6. Taylor, M., & Prendergast, P. J. (2015). Four decades of finite element analysis of orthopaedic devices: Where are we now and what are the opportunities? *Journal of Biomechanics, 48*(5), 767–778. https://doi.org/10.1016/j.jbiomech.2014.12.019
7. Aldieri, A., Terzini, M., Osella, G., Priola, A. M., Angeli, A., Veltri, A., Audenino, A., & Bignardi, C. (2018). Osteoporotic hip fracture prediction: Is T-score-based criterion enough? A hip structural analysis-based model. *Journal of Biomechanical Engineering*. https://doi.org/10.1115/1.4040586
8. Aldieri, A., Terzini, M., Audenino, A. L., Bignardi, C., Paggiosi, M., Eastell, R., Viceconti, M., & Bhattacharya, P. (2022). Personalised 3D assessment of trochanteric soft tissues improves HIP fracture classification accuracy. *Annals of Biomedical Engineering, 50*(3), 303–313. https://doi.org/10.1007/s10439-022-02924-1
9. Benemerito, I., Griffiths, W., Allsopp, J., Furnass, W., Bhattacharya, P., Li, X., Viceconti, M., & Narracott, A. (2021). Delivering computationally-intensive digital patient applications to the clinic: An exemplar solution to predict femoral bone strength from CT data. *Computer Methods and Programs in Biomedicine, 208*, 106–200. https://doi.org/10.1016/j.cmpb.2021.106200
10. Huppertz, A., Radmer, S., Asbach, P., Juran, R., Schwenke, C., Diederichs, G., Viceconti, M., & Sparmann, M. (2011). Computed tomography for preoperative planning in minimal-invasive total hip arthroplasty: Radiation exposure and cost analysis. *European Journal of Radiology, 78*(3), 406–413. https://doi.org/10.1016/j.ejrad.2009.11.024
11. O'Toole, R. V., Jaramaz, B., DiGioia, A. M., Visnic, C. D., & Reid, R. H. (1995). Biomechanics for preoperative planning and surgical simulations in orthopaedics. *Computers in Biology and medicine, 25*(2), 183–191. https://doi.org/10.1016/0010-4825(94)00043-p
12. Terzini, M., Aldieri, A., Rinaudo, L., Osella, G., Audenino, A. L., & Bignardi, C. (2019). Improving the hip fracture risk prediction through 2D finite element models from DXA images: Validation against 3D models. *Frontiers in Bioengineering and Biotechnology*. https://doi.org/10.3389/fbioe.2019.00220
13. Dall'Ara, E., Eastell, R., Viceconti, M., Pahr, D., & Yang, L. (2016). Experimental validation of DXA-based finite element models for prediction of femoral strength. *Journal of the Mechanical Behavior of Biomedical Materials, 63*, 17–25. https://doi.org/10.1016/j.jmbbm.2016.06.004
14. Ulivieri, F. M., & Rinaudo, L. (2021). Beyond bone mineral density: A new dual X-ray absorptiometry index of bone strength to predict fragility fractures, the bone strain index. *Frontiers in Medicine*. https://doi.org/10.3389/fmed.2020.590139
15. Colombo, C., Libonati, F., Rinaudo, L., Bellazzi, M., Ulivieri, F. M., & Vergani, L. (2019). A new finite element based parameter to predict bone fracture. *PLoS ONE*. https://doi.org/10.1371/journal.pone.0225905
16. Heyland, M., Checa, S., Kendoff, D., & Duda, G. N. (2019). Anatomic grooved stem mitigates strain shielding compared to established total hip arthroplasty stem designs in finite-element models. *Scientific Reports, 9*(1), 1–11. https://doi.org/10.1038/s41598-018-36503-z
17. Oshkour, A. A., Osman, N. A. A., Yau, Y. H., Tarlochan, F., & Abas, W. A. B. W. (2013). Design of new generation femoral prostheses using functionally graded materials: A finite element analysis. *Proceedings of the Institution of Mechanical Engineers, Part H: Journal of Engineering in Medicine, 227*(1), 3–17. https://doi.org/10.1177/0954411912459421
18. Reimeringer, M., & Nuño, N. (2016). The influence of contact ratio and its location on the primary stability of cementless total hip arthroplasty: A finite element analysis. *Journal of Biomechanics, 49*(7), 1064–1070. https://doi.org/10.1016/j.jbiomech.2016.02.031
19. MatWeb L.L.C (2022). *Matweb: material property data*. Retrieved May 31, 2022, from http://www.matweb.com/
20. Ramaniraka, N. A., Rakotomanana, L. R., & Leyvraz, P.-F. (2000). The fixation of the cemented femoral component. *The Journal of Bone and Joint Surgery British, 82-B*(2), 297–303. https://doi.org/10.1302/0301-620x.82b2.0820297
21. Naylor, K. E., McCloskey, E. V., Eastell, R., & Yang, L. (2013). Use of DXA-based finite element analysis of the proximal femur in a longitudinal study of hip fracture. *Journal of Bone and Mineral Research, 28*(5), 1014–1021. https://doi.org/10.1002/jbmr.1856
22. Morgan, E. F., Bayraktar, H. H., & Keaveny, T. M. (2003). Trabecular bone modulus-density relationships depend on anatomic site. *Journal of Biomechanics, 36*(7), 897–904. https://doi.org/10.1016/S0021-9290(03)00071-X
23. Quevedo Gonzalez, F. J., Reimeringer, M., & Nuno, N. (2017). On the two-dimensional simplification of three-dimensional cementless hip stem numerical models. *Journal of Biomechanical Engineering*. https://doi.org/10.1115/1.4035368
24. Fernandes, P. R., Folgado, J., & Ruben, R. B. (2004). Shape optimization of a cementless hip stem for a minimum of interface stress and displacement. *Computer Methods in Biomechanics and Biomedical Engineering, 7*(1), 51–61. https://doi.org/10.1080/10255840410001661637
25. Janssen, D., van Aken, J., Scheerlinck, T., & Verdonschot, N. (2009). Finite element analysis of the effect of cementing concepts on implant stability and cement fatigue failure. *Acta Orthopaedica, 80*(3), 319–324. https://doi.org/10.3109/17453670902947465
26. Wong, A. S., New, A. M. R., Isaacs, G., & Taylor, M. (2005). Effect of bone material properties on the initial stability of a cementless hip stem: A finite element study. *Proceedings of the Institution of Mechanical Engineers, Part H: Journal of Engineering in Medicine, 219*(4), 265–275. https://doi.org/10.1243/095441105X34293
27. Heller, M. O., Bergmann, G., Kassi, J. P., Claes, L., Haas, N. P., & Duda, G. N. (2005). Determination of muscle loading at the hip joint for use in pre-clinical testing. *Journal of Biomechanics, 38*(5), 1155–1163. https://doi.org/10.1016/j.jbiomech.2004.05.022
28. Chong, D. Y. R., Hansen, U. N., & Amis, A. A. (2010). Analysis of bone-prosthesis interface micromotion for cementless tibial prosthesis fixation and the influence of loading conditions. *Journal of Biomechanics, 43*(6), 1074–1080. https://doi.org/10.1016/j.jbiomech.2009.12.006

29. Viceconti, M., Monti, L., Muccini, R., Bernakiewicz, M., & Toni, A. (2001). Even a thin layer of soft tissue may compromise the primary stability of cementless hip stems. *Clinical Biomechanics, 16*(9), 765–775. https://doi.org/10.1016/s0268-0033(01)00052-3
30. Huiskes, R., Weinans, H. H. J. G., Grootenboer, H. J., Dalstra, M., Fudala, B., & Slooff, T. J. (1987). Adaptive bone-remodeling theory applied to prosthetic-design analysis. *Journal of Biomechanics, 20*(11–12), 1135–1150. https://doi.org/10.1016/0021-9290(87)90030-3
31. Chen, Z., Jin, L., Wang, W., & Zhou, J. (2021). Pre-operative bone mineral density is a predictive factor for excellent early patient-reported outcome measures in cementless total hip arthroplasty using a proximally fixed anatomic stem. A prospective study at two year minimum follow-up: several questions. *International Orthopaedics, 45*(5), 1383–1384. https://doi.org/10.1007/s00264-020-04886-2
32. Wilkinson, J. M., Hamer, A. J., Rogers, A., Stockley, I., & Eastell, R. (2003). Bone mineral density and biochemical markers of bone turnover in aseptic loosening after total hip arthroplasty. *Journal of Orthopaedic Research, 21*(4), 691–696. https://doi.org/10.1016/S0736-0266(02)00237-1
33. Hua, J., & Walker, P. S. (1992). A comparison of cortical strain after cemented and press-fit proximal and distal femoral replacement. *Journal of Orthopaedic Research, 10*(5), 739–744. https://doi.org/10.1002/jor.1100100516
34. Huiskes, R. (1993). Failed innovation in total hip replacement. Diagnosis and proposals for a cure. *Acta Orthopaedica Scandinavica, 64*(6), 699–716. https://doi.org/10.3109/17453679308994602
35. Huiskes, R. (1990). The various stress patterns of press-fit, ingrown, and cemented femoral stems. *Clinical Orthopaedics and Related Research, 261*, 27–38.
36. Tecnologie Avanzate T. A. (2022). *Bone Strain Index*. Retrieved May 31, 2002, from https://tecnologieavanzate.com/en/research-and-development/bone-strain-index/
37. Zotov, E., Hills, A. F., de Mello, F. L., Aram, P., Sayers, A., Blom, A. W., Wilkinson, J. M., & Kadirkamanathan, V. (2020). JointCalc: A web-based personalised patient decision support tool for joint replacement. *International Journal of Medical Informatics*. https://doi.org/10.1016/j.ijmedinf.2020.104217

Authors and Affiliations

Sofia Cuttone[1] · Luca Rinaudo[1] · Cristina Bignardi[2,3] · Alessandra Aldieri[4,5] · Mara Terzini[2,3] · Antonio Croce[6] · Carmelo Messina[6] · Laura Mangiavini[6,7] · Luca Maria Sconfienza[6,7] · Fabio Massimo Ulivieri[8]

Sofia Cuttone
sofia.cuttone@icloud.com

Luca Rinaudo
l3rinaudo@gmail.com

Cristina Bignardi
cristina.bignardi@polito.it

Alessandra Aldieri
alessandra.aldieri@polito.it

Mara Terzini
mara.terzini@polito.it

Antonio Croce
antoniocro@libero.it

Carmelo Messina
carmelomessina.md@gmail.com

Laura Mangiavini
laura.mangiavini@unimi.it

Luca Maria Sconfienza
luca.sconfienza@unimi.it

1 Tecnologie Avanzate T.A. s.r.l, Lungo Dora Voghera 36/A, Turin, Italy

2 PolitoBIOMed Lab, Department of Mechanical and Aerospace Engineering, Politecnico di Torino, Corso Duca degli Abruzzi 24, Turin, Italy

3 Department of Mechanical and Aerospace Engineering, Politecnico di Torino, Turin, Italy

4 Department of Industrial Engineering, Alma Mater Studiorum - University of Bologna, Bologna, Italy

5 Laboratorio di Tecnologia Medica, IRCCS Istituto Ortopedico Rizzoli, Bologna, Italy

6 IRCCS Istituto Ortopedico Galeazzi, Via Riccardo Galeazzi 4, Milan, Italy

7 Department of Biomedical Sciences for Health, University of Milan, Milan, Italy

8 Bone Metabolic Unit, Casa di Cura La Madonnina, Via Quadronno 29, Milan, Italy